

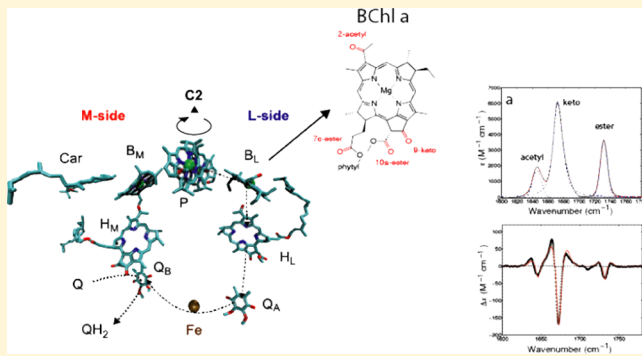
Local and Global Electric Field Asymmetry in Photosynthetic Reaction Centers

Miguel Saggi,[†] Stephen D. Fried,[‡] and Steven G. Boxer*^{†,ID}

Department of Chemistry, Stanford University, Stanford, California 94305-5080, United States

 Supporting Information

ABSTRACT: The origin of unidirectional electron transfer in photosynthetic reaction centers (RCs) has been widely discussed. Despite the high level of structural similarity between the two branches of pigments that participate in the initial electron transfer steps of photosynthesis, electron transfer only occurs along one branch. One possible explanation for this functional asymmetry is the differences in the electrostatic environment between the active and the inactive branches arising from the charges and dipoles of the organized protein structure. We present an analysis of electric fields in the RC of the purple bacterium *Rhodobacter sphaeroides* using the intrinsic carbonyl groups of the pigments as vibrational reporters whose vibrational frequency shifts can be converted into electric fields based on the vibrational Stark effect and also provide Stark effect data for plant pigments that can be used in future studies. The carbonyl stretches of the isolated pigments show pronounced Stark effects. We use these data, solvatochromism, molecular dynamics simulations, and data in the literature from IR and Raman spectra to evaluate differences in fields at symmetry-related positions, in particular at the 9-keto and 2-acetyl positions of the pigments involved in primary charge separation.



1. INTRODUCTION

The primary charge separation steps of photosynthesis occur in the reaction center (RC),¹ a protein complex that consists of three polypeptides (denoted as H, L, and M subunits), which encases 9 pigments and a nonheme iron in a precise configuration. The photosynthetic pigments comprise four bacteriochlorophylls (P_L , P_M , B_L , and B_M), two bacteriopheophytins (H_L and H_M), two quinones (Q_A and Q_B), and one carotenoid (Figure 1a; an alternative notation replaces L with A and M with B).^{2,3} Crystal structures from RCs of the purple bacteria *Rhodobacter sphaeroides* and *Blastochloris viridis* were solved at high resolution in the 1990s² and show the presence of an approximate local C_2 symmetry axis between the L and M subunits. Two of the bacteriochlorophylls are arranged in close proximity, forming the special pair (P) that serves as the primary electron donor. The other two bacteriochlorophylls (B_L and B_M) and the bacteriopheophytins (H_L and H_M) are located in two branches on either side of the pseudosymmetry axis (denoted the L-side and M-side or alternatively the A and B side, respectively). A very similar overall chromophore organization is found in both photosystem I (PS I) and photosystem II (PS II) RCs in green plants and cyanobacteria, where chlorophyll *a* replaces bacteriochlorophyll *a* (BChl *a*).

The process of charge separation starts either by energy transfer from the antenna system to the special pair or by direct absorption of light forming the excited state P^* .⁴ P^* decays in 3–4 ps by electron transfer (ET) to $P^+H_L^-$. From H_L^- , the

electron moves to Q_A in about 200 ps to form $P^+Q_A^-$.⁵ The electron is then passed from Q_A^- to Q_B on a time scale of 100 μ s, forming a semiquinone on the Q_B site. B_L plays a significant role in mediating ultrafast ET, though if it is ever reduced, it is, at most, transiently formed.^{4,6}

Despite the chemical and structural similarity of the L- and M-branch ET pathways, ET in bacterial RCs occurs predominantly along the L-branch (a ~65:1 ratio).⁴ Understanding the origin(s) of this functional symmetry breaking has been a major challenge for investigators working in the field. Many proposals have been advanced to explain this unidirectional ET, for example, differences in the electronic coupling between cofactors in the L- and M-branches, differences in relative free energies of initial charge-separated intermediates (e.g., $P^+B_L^-$ vs $P^+B_M^-$), asymmetry in the dielectric environments of both branches, or asymmetry in the protein electrostatic or matrix electric fields.^{7–9} With respect to the latter point, an early proposal is that the arrangement of protein charges and dipoles creates a potential gradient that favors the charge separation between chromophores on the L side ($P^* \rightarrow P^+H_L^-$) over the M side ($P^* \rightarrow P^+H_M^-$). Calculated electrostatic free energies indicate that ET via H_L is favored by 0.8 eV compared to 0.4 eV via H_M , based on the *B*.

Received: November 27, 2018

Revised: January 13, 2019

Published: January 22, 2019

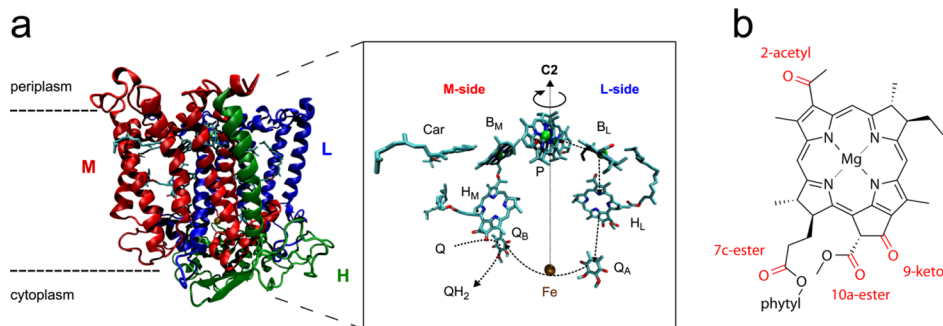


Figure 1. (a) Crystal structure of the photosynthetic RC from *Rb. sphaeroides* with the prosthetic groups arranged in a C-2 symmetry (pdb entry 1PCR). (b) Structure of BChl *a* with highlighted carbonyl groups.

viridis crystal structure.¹⁰ However, there has previously been no experimental means to test the calculated differences in electric fields between the L and M sides.

Measurements of electric fields in proteins and model systems based on the vibrational Stark effect have gained attention recently because of the minimal structural perturbation introduced by vibrational reporter groups.¹¹ Much of the work on proteins has utilized diatomic probes such as nitriles because their vibrational modes occur in a spectral window that is, free of any interfering protein modes, while possessing reasonably large extinction coefficients.^{12–14} Nitriles can be introduced on inhibitors (drugs), by site-specific labeling of cysteines as thiocyanates (–SCN), semisynthetically by the introduction of peptides containing noncanonical amino acids or by amber suppression.^{13–15} Despite extensive efforts in our lab, it has proved very difficult to place thiocyanate probes in symmetry-related positions near to the functional chromophores in bacterial RCs;^{16,17} the recent development of amber suppression in *Rb. sphaeroides* should facilitate the introduction of spectator IR probes.¹⁸

In this work, we use the intrinsic carbonyl groups of the pigments inside the RC as reporters of electric fields. As seen in Figure 1b, BChl *a*, and bacteriopheophytin *a* (BPhe *a*) each contain 4 carbonyl groups, the 9-keto and 2-acetyl groups, which are part of the conjugated π -system of the macrocycles, an ester at position 10, and the 7c-ester group next to the phytol side chain. Unlike the electronic transitions of the chromophores, which are coupled to each other,^{19,20} the carbonyl groups are relatively isolated and offer ideal probes for estimating the projection of the protein electric field on symmetry-related positions. The vibrational frequencies of the carbonyl groups of the chromophores inside the protein have been assigned in previous work, mainly for *Rb. sphaeroides*, using Fourier transform infrared (FTIR) difference (light-minus-dark) and resonance Raman spectroscopy, and assigned by site-directed mutagenesis that introduced or removed hydrogen bonds to the carbonyls or by wavelength-specific resonance enhancement.^{21–23} Following a strategy we have developed elsewhere,^{13,24,25} we first measure the sensitivity of each vibration in the isolated chromophores to an external electric field using vibrational Stark spectroscopy giving the Stark tuning rate, $|\Delta\tilde{\mu}_{C=O}|$, a measure of the sensitivity of the vibrational transition to an electric field. This is combined with solvatochromism data and molecular dynamics (MD) simulations to produce a calibrated frequency-field conversion. We then use these data to evaluate the difference in field $\vec{F}_L - \vec{F}_M = \Delta\vec{F}_{L-M}$ sensed by each of the intrinsic carbonyl probes at symmetry-related positions on the L and M side of

the RC based on observed frequency differences, $\Delta\tilde{v}_{\text{L-M}}^{\text{obs}} = \Delta\vec{\mu}_{\text{C=O}} \cdot \Delta\vec{F}_{\text{L-M}}$, to determine whether there is any evidence for a large difference in the electric field sensed by these probes beyond the local and specific effects of hydrogen bonds. Note that the units we use for the electric field are MV/cm, and for Stark tuning rates, $\text{cm}^{-1}/(\text{MV}/\text{cm})$. Because both the Stark tuning rate and the field are vector quantities, their relative orientations enter as the dot product for a linear Stark effect. $\Delta\vec{\mu}_{\text{C=O}}$ is typically parallel to the carbonyl transition dipole moment that in turn is parallel to the C=O bond axis.¹⁶ The frequency-field calibration also provides an estimate for the absolute value of the fields sensed at different positions, though we will be primarily interested in differences between the L and M sides in the following.

As mentioned above, earlier work from our lab using electronic Stark spectroscopy revealed a difference in dielectric screening of the $P^+Q_A^-$ dipole sensed by a difference in Q_A^- electronic spectral shift of the B_L versus B_M and H_L versus H_M , giving effective dielectric constants ϵ_{eff} around the chromophores, which are in the range of $\epsilon_{\text{eff}} = 1.5-2.5$ for the M-side and $\epsilon_{\text{eff}} = 4.5-9.5$ for the L-side.⁸ Effective dielectric constants in this case describe the ratio between calculated electronic band shifts in vacuum and observed band shifts in frozen solution ($\epsilon_{\text{eff}} = \Delta\nu_{\text{calc}}(\epsilon = 1)/\Delta\nu_{\text{obs}}$). However, there can be electronic coupling between the chromophores, which influences the electronic spectra and could complicate analysis.⁷ In addition, the experimental quantification of electric fields from the UV/vis spectra is limited based on the fact that the exact orientation of the electronic difference dipole is not known with certainty. Vibrational spectroscopy in this work offers the advantage that the difference dipoles of carbonyl groups are always co-linear to the $C=O$ bond and their orientation is known from the crystal structure. Furthermore, the field difference, if any, sensed by these vibrational probes is the intrinsic field difference due to the organized environment around the reactive components in the ground state before any charge separation.

2. MATERIALS AND METHODS

2.1. Extraction and Purification of Photosynthetic

Pigments. *Rb. capsulatus* cells were grown semi aerobically as described previously.²⁶ Cells were harvested and lyophilized after addition of 8 mM trehalose. For extraction of pigments, the lyophilized cells were resuspended in a mixture of methanol/ethyl ether/petroleum ether (5:2:1 v/v).²⁷ A second extraction with methanol/ethyl ether (5:2 v/v) was performed and both fractions were combined, and 10% NaCl solution was added until phase separation occurred. The ether phase, which

contained the BChl *a* and other hydrophobic pigments, was washed with 10% NaCl solution and dried under vacuum. Pigments were dissolved in 1 mL HPLC solvent (see below) and filtered through a 0.22 μm nylon filter. Purification was carried out using a semi-prep-scale C18 column (Agilent Zorbax 300SB C18, 9.4 \times 250 mm, 5 μm) and a multiple wavelength detector (1260 MWD VL). Pigments were detected at 770 nm using isocratic elution with acetonitrile/ethyl acetate/MeOH/water (24:20:47:9 v/v) as the mobile phase at a flow rate of 5 mL/min. The fraction containing BChl *a* was dried under vacuum and stored at -80°C until further use. BPhe *a* was obtained by the addition of 3% concentrated HCl to BChl *a*. After color change, diethyl ether and water were added, and the ether layer was washed with water until the acid was removed, and the mixture was repurified on HPLC under the same conditions.

Chlorophylls were extracted from fresh spinach by the addition of methanol. The solution was filtered and 1,4-dioxane was added (1:7 v/v).²⁸ Water was added dropwise until turbidity increased and the solution was placed in a -20°C freezer for 20 min. During this time, chlorophyll *a* and *b* (Chl *a* and *b*) precipitated out as dioxane complexes and were collected by centrifugation. The precipitate was dissolved in 1 mL HPLC solvent, filtered, and loaded onto HPLC. Separation of chlorophyll *a/b* was achieved using the same HPLC setup as described above but with acetonitrile/methanol/ethyl acetate (53:40:7 v/v) as the mobile phase. Pigments were detected at 660 nm using isocratic elution at a flow-rate of 5 mL/min. Pheophytin *a* (Pheo *a*) was obtained by the addition of a few drops of 1 N hydrochloric acid to a solution of Chl *a* in acetone. After color change, diethyl ether and water were added and the ether layer was washed with water until the acid was removed. The sample was repurified on HPLC. The purity of all studied pigments was confirmed by HPLC and UV/vis absorption spectroscopy and was $>99\%$.²⁷

Samples of ubiquinone (Q_{10}) and vitamin K₁ were purchased from Sigma-Aldrich at the highest available purity ($>98\%$).

2.2. Vibrational Spectroscopy. All spectra were recorded on a Bruker Vertex 70 FTIR spectrometer equipped with a liquid nitrogen-cooled MCT detector at a spectral resolution of 1 cm^{-1} . For solvatochromism measurements, pigments were dissolved in organic solvents to a concentration of 2–5 mM. For chlorophyll samples, 6 equivalents of pyridine were added in order to maintain a defined coordination shell around the Mg atom and so the pigments were monomeric in a range of bulk solvents. Vibrational spectra were obtained at room temperature by averaging 64 scans and subtracting a reference spectrum consisting of neat solvents without pigments. For vibrational Stark spectroscopy, measurements were carried out at low temperature using a home-built cryostat.²⁹ A small amount of the sample ($\sim 4 \mu\text{L}$) was loaded into a home-built cell with two CaF_2 windows (thickness 1 mm, diameter 13 mm, Red Optronics, Mountain View, CA). The windows were coated with a 45 \AA Ni layer on the inside to function as a capacitor and separated by two Teflon spacers of 26 μm thickness. Samples were frozen rapidly in liquid nitrogen into organic glasses using 2-methyltetrahydrofuran (2-methyl-THF) or a mixture of dichloromethane/dichloroethane (DCM/DCE, 1:3 v/v). A high-power voltage supply was connected to the cell (Trek Instruments Inc., Medina, NY) and the output voltage was synchronized with the FTIR scanning time. Spectra were acquired in the rapid scan mode and the

resulting Stark spectra were the difference between 512 spectra recorded in the presence of an applied field minus 512 spectra recorded under identical conditions without the field.³⁰ As a control, spectra were recorded at multiple electric field strengths to confirm that the Stark signals scale quadratically with the field strength, as expected for an isotropic, immobilized sample.³⁰ To obtain the Stark tuning rates $|\Delta\vec{\mu}\cdot\vec{f}|$, where *f* is the local field correction factor,³¹ the spectra were fitted using the in-house written program SpectFit.³² Because most spectra had overlapping bands, a fitting procedure has been applied in which the absorption and Stark spectra were fit simultaneously, as described previously.³⁰

2.3. Solvatochromism and Electric Field Calculations.

To model solvent-induced frequency shifts in terms of electric fields and to develop field-frequency calibration curves, we calculated the solvent reaction fields that several organic solvents (cyclohexane, ether, THF, pyridine, acetonitrile, dimethyl sulfoxide (DMSO), chloroform, and DCM) exert onto the carbonyl groups (keto, acetyl, and esters) of BChl *a*, BPhe *a*, Chl *a*, and Pheo *a* by MD simulations. The parameters for Chl *a* and Pheo *a* were taken from Zhang et al.³³ who used an AMBER03-like method to obtain the charges. Valence parameters were derived from previous work by Ceccarelli et al.³⁴ The bacteriochlorophyll pigments differ from the chlorophyll pigments in two ways: the vinyl group on ring I is replaced with an acetyl group and ring II lacks a degree of unsaturation between atoms C2 and C3 (Figure 1b). In developing models for BChl *a* and BPhe *a*, we opted to maintain much of the parameterization from Zhang and Friesner's work.⁷ Using the existing atom types, all necessary bond and angle valence terms were described. Five improper dihedral terms were missing, and their values were inferred by comparison to the closest analogues present in Zhang and Friesner's parameter set (see full parameters in the *Supporting Information*). Charges were maintained from Zhang and Friesner except for atoms on the acetyl group, C2 and C3 on ring II, and their hydrogens. The charges for the acetyl group were taken from Ceccarelli.³⁴ For C2 and C3, the original charge was divided equally among the carbon and the new hydrogen atom bound to it. Generalized AMBER parameters (GAFF) to model the solvent molecules were taken from the virtualchemistry.org database.³⁵

We simulated solutions consisting of 1500–3000 solvent molecules (to fill a 65 \AA cubic box) and 1 pigment molecule and calculated the electric field the solvent projected onto the bond axes of the various C=O bonds of the pigment using methods similar to those previously described.³⁶ Solvent boxes were first equilibrated for 100 ps at 150 K and then at 300 K in an *NPT* ensemble. Production dynamics evolved the solvation simulations for 2 further ns, during which the solvent field on the carbonyl groups was calculated every 200 fs. Solvent fields compiled in Table S1 refer to their average values over the production trajectories (the distribution of fields is related to inhomogeneous broadening of the vibrational transitions).²⁵

3. RESULTS

3.1. Vibrational Stark Spectroscopy of Bacterial Pigments. The carbonyl stretching modes of BChl *a* and BPhe *a* have been assigned in the literature for the isolated pigments *in vitro* as well as embedded in RCs (mostly for *Rb. sphaeroides*). The vibrational modes of the carbonyls are well separated and the ester modes usually occur between 1750 and 1720 cm^{-1} , the 9-keto mode between 1710 and 1670 cm^{-1} ,

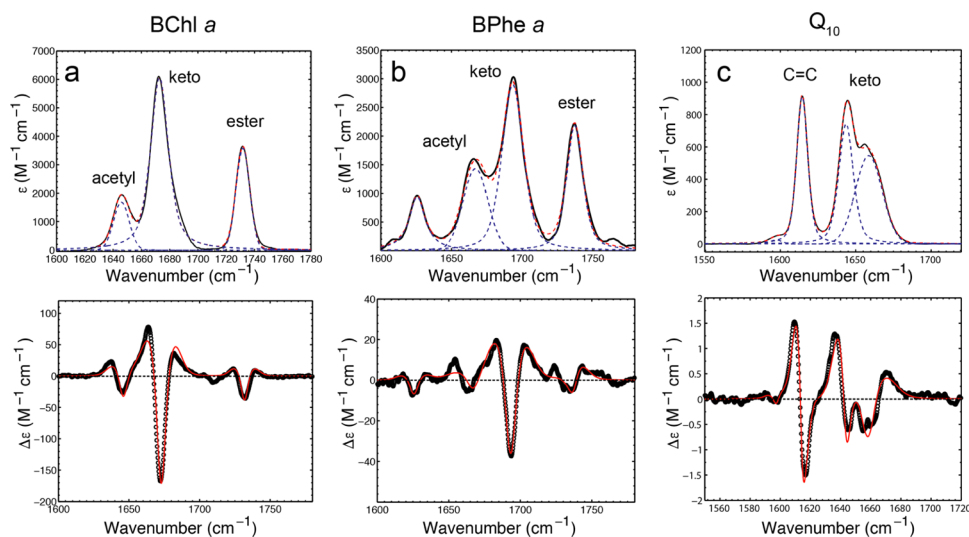


Figure 2. FTIR spectra in the carbonyl region (upper) and vibrational Stark spectra (lower) of photosynthetic chromophores at $T = 77$ K. (a) 5 mM BChl *a* in 2-methyl-THF; (b) 4.4 mM BPhe *a* in 2-methyl-THF; (c) 50 mM Q_{10} in DCM/DCE. Vibrational Stark spectra are overlaid with best fits shown in red giving $|\Delta\vec{\mu}|f$ (see Table 1). Stark spectra are shown scaled to an external field of 1 MV/cm.

Table 1. Vibrational Frequencies, Extinction Coefficients, and Stark Tuning Rates Extracted from the Fittings of the Experimental Data in Figure 2 (Figure S1 for Green Plant Pigments)

molecule	carbonyl	$\bar{\nu}$ (cm ⁻¹)	ϵ (M ⁻¹ cm ⁻¹)	$ \Delta\vec{\mu} f$ [cm ⁻¹ /(MV/cm)]
BChl <i>a</i> ^a	9-keto	1672	6100	3.1 ± 0.3
	2-acetyl	1646	1950	2.3 ± 0.2
	ester	1732	3650	1.4 ± 0.2
BPhe ^a	9-keto	1694	3100	2.7 ± 0.3
	2-acetyl	1666	1600	1.8 ± 0.3
	ester	1737	2200	1.2 ± 0.2
ubiquinone Q_{10} ^b	C ₁ -keto/C ₄ -keto	1659/1644	550/740	$0.99 \pm 0.03/0.95 \pm 0.03$
	C=C	1615	910	0.60 ± 0.03
Chl <i>a</i> ^a	13-keto	1679	3300	2.6 ± 0.2
	ester	1733	2700	1.4 ± 0.2
Pheo <i>a</i> ^a	13-keto	1699	3100	2.1 ± 0.2
	ester	1733	2300	1.0 ± 0.1
vitamin K ₁ ^b	keto	1659/1653	690/630	0.65 ± 0.03
	C=C	1592	110	0.53 ± 0.03

^a2Me-THF at $T = 77$ K. ^bDCM/DCE at $T = 77$ K

and the 2-acetyl mode between 1650 and 1620 cm⁻¹.^{21,27,37} Note that the ester modes are indistinguishable in many solvents, but they can be different when the chromophore is embedded inside the protein because of the anisotropic nature of the environment.²¹

The low-temperature FTIR spectra of BChl *a* and BPhe *a* dissolved in 2-methyl-THF are shown in Figure 2a,b. The peaks for the 9-keto, the 2-acetyl and the ester modes are well resolved at 1672, 1646, and 1732 cm⁻¹, respectively (Table 1). The transitions have large extinction coefficients (>2000 M⁻¹ cm⁻¹), suggesting large Stark tuning rates, as studies on other vibrational groups have shown a correlation between $|\Delta\vec{\mu}|f$ and the transition moment (see below).^{30,38}

To study the intrinsic sensitivity of the different carbonyl modes to an electric field, we performed vibrational Stark spectroscopy. In general, all vibrational Stark spectra obtained for model systems of carbonyls so far are dominated by the linear Stark effect, that is, the difference polarizabilities $\Delta\bar{\alpha}$ that give rise to quadratic Stark effects are negligible.³⁹ Consistent with this, the vibrational Stark spectra of BChl *a* and BPhe *a*

show clearly resolved features, dominated by a second derivative of absorption contribution, which allows robust fitting of the data. Because some of the bands partially overlap, we simultaneously fitted the absorption and Stark spectra with the same data set allowing for a more accurate analysis.³⁰ The 9-keto group of BChl *a* exhibits the largest Stark effect with a Stark tuning rate of $|\Delta\vec{\mu}|f = 3.1$ cm⁻¹/(MV/cm), the largest tuning rate observed for a carbonyl group to date (Table 1).^{24,39} The Stark tuning rates for the 2-acetyl and ester groups are smaller with $|\Delta\vec{\mu}|f = 2.3$ cm⁻¹/(MV/cm) and $|\Delta\vec{\mu}|f = 1.4$ cm⁻¹/(MV/cm), respectively. Note that the local field correction factor, treated here as a scalar, f , gives the difference between the applied field and the actual field felt by the chromophore being probed. Its value is not certain, but is likely around $f \approx 2$.²⁵ Because of this uncertainty, Stark tuning rates are reported as $|\Delta\vec{\mu}|f$. A similar pattern is observed for BPhe *a*, with all vibrational modes exhibiting slightly smaller Stark tuning rates (Figure 2b). In the Discussion section, we use these experimental values of $|\Delta\vec{\mu}|f$ as part of a quantitative analysis of the electric fields in the RC of *Rb. sphaeroides*.

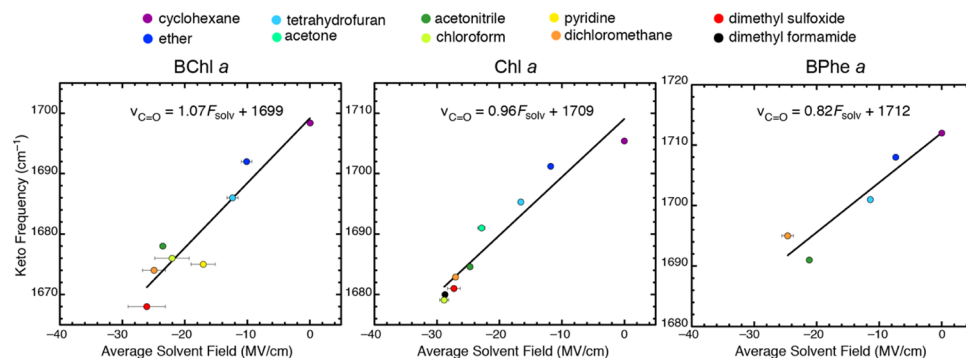


Figure 3. Plots of 9-keto frequencies of pigments dissolved in organic solvents compared against the average electric field the 9-keto group experiences in each of those solvents, calculated by MD simulation.

For completeness, we also studied ubiquinone Q_{10} dissolved in DCM/DCE (Figure 2c). The FTIR spectrum shows two peaks corresponding to the C_1^- and the C_4 -keto groups at 1659 and 1644 cm^{-1} and another clearly resolved band around 1610 cm^{-1} , which can be attributed to the $C=C$ stretch.⁴⁰ The extinction coefficients are much smaller compared to BChl *a* and BPhe *a*, which is reflected in a smaller Stark tuning rate as well (see below). The Stark spectrum shows three resolved features with Stark tuning rates around $|\Delta\vec{\mu}\cdot\vec{f}| \approx 1.0\text{ cm}^{-1}/(\text{MV/cm})$ for the keto groups and $|\Delta\vec{\mu}\cdot\vec{f}| \approx 0.6\text{ cm}^{-1}/(\text{MV/cm})$ for the $C=C$ stretch. This value is similar to previously reported values for other carbonyl-containing molecules.^{24,36} The Stark effect of the $C=C$ stretch is surprisingly large, most likely because this mode is coupled to both keto modes.⁵

3.2. Vibrational Stark Spectroscopy of Plant Pigments. To obtain a complete dataset for the most common pigments in photosynthetic systems and as a comparison to oxygenic photosynthesis, we obtained data for Chl *a* and Pheo *a*. One difference between BChls and Chls is that the latter pigments are missing the 2-acetyl group, which is replaced by a vinyl group. For this reason, the vibrational spectra in the carbonyl region are less complex. Note also that the atom numbering for Chl is different and that the 9-keto group of BChl corresponds to the 13-keto group of Chl. Figure S1 shows the FTIR and vibrational Stark spectra of Chl *a* and Pheo *a* dissolved in 2-methyl-THF and Table 1 lists vibrational frequencies, extinction coefficients, and vibrational Stark tuning rates for the carbonyl groups. As seen for BChl *a*, the largest Stark effect for Chl *a* arises from the 13-keto group and is of comparable magnitude with $|\Delta\vec{\mu}\cdot\vec{f}| \approx 2.6\text{ cm}^{-1}/(\text{MV/cm})$. Removing the central Mg atom and transforming Chl *a* into Pheo *a* results in a smaller Stark effect with $|\Delta\vec{\mu}\cdot\vec{f}| \approx 2.1\text{ cm}^{-1}/(\text{MV/cm})$, in analogy to BChl *a* versus BPhe *a*.

PS II contains plastoquinone, which has a very similar structure to ubiquinone and is expected to show a comparable Stark effect to ubiquinone. A variety of quinones can be found in photosystems of plants, most of their derivatives of benzoquinone or 1,4-naphthoquinone. Therefore, we performed vibrational Stark experiments on vitamin K₁, which is a derivative of 1,4-naphthoquinone, and can be found in PS I. Vitamin K₁ shows three main bands in the region between 1600 and 1700 cm^{-1} .⁴⁰ The bands of the two keto modes can be seen at 1659 and 1653 cm^{-1} ; in the lower frequency region, two more bands from the aromatic $C=C$ stretch at 1620 cm^{-1} and the quinone $C=C$ stretch at 1595 cm^{-1} are found. The corresponding vibrational Stark spectra are shown in Figure S1. Vitamin K₁ shows a smaller Stark effect than ubiquinone with

the Stark tuning rates $|\Delta\vec{\mu}\cdot\vec{f}| \approx 0.65\text{ cm}^{-1}/(\text{MV/cm})$ for the carbonyl stretch and $|\Delta\vec{\mu}\cdot\vec{f}| \approx 0.53\text{ cm}^{-1}/(\text{MV/cm})$ for the $C=C$ stretch. As seen for ubiquinone, the $C=C$ stretch shows a comparable Stark effect to the keto groups, most likely because of an admixture of the carbonyl stretch.

3.3. Solvatochromism and Frequency-Field Calibration Curves. Following earlier work, we recorded the IR spectra of Chl *a*, BChl *a*, Pheo *a*, and BPhe *a* in a variety of organic solvents ranging in polarity from cyclohexane to DMSO (the pigments are not soluble in water); the frequencies are compiled in Table S1. Note that for the Mg-containing pigments, several equivalents of pyridine were added to ensure that the pigments were monomeric, avoiding as much as possible aggregates where carbonyl groups from one molecule form complexes with the central Mg atom of another (an interaction that does not occur in RCs; note that the pyridine moieties were not included in the simulations). As has been found for many carbonyl vibrations,⁴¹ we observed consistent red shifts of the carbonyl bands with increased solvent polarity. Using MD simulations to model the solvation environment and calculate solvent reaction fields, we found that solvatochromic trends were well explained in terms of a linear Stark effect.³⁶ This enabled us to use solvatochromism measurements as reference data to establish field-frequency calibration curves, which extends the vibrational Stark effect method by mapping particular frequencies to absolute electric fields. In the following, we applied this concept to the photosynthetic pigments. The electric fields for the carbonyl groups of all 4 pigments dissolved in 8 different solvents are compiled in Table S2; Figure 3 presents the more significant results.

In general, the 9-keto vibration provided the most robust field-frequency curves with R^2 -values clustered around 0.90, and these are displayed in Figure 3. The slope corresponds to the vibration's sensitivity to solvent field, and the intercept to the vibration's frequency in zero electric field. For BChl *a* (Figure 3a), the slope's value [$1.1 \pm 0.15\text{ cm}^{-1}/(\text{MV/cm})$] is (2.8 ± 0.6) -fold smaller than the observed Stark tuning rate [$3.1 \pm 0.3\text{ cm}^{-1}/(\text{MV/cm})$]. A difference in this range has been observed for all other carbonyl vibrations investigated to date³⁰ and is believed to reflect—at least partially—the local field effect, that is, present when an external field is used (i.e., $f \approx 2$), but not for solvatochromism.⁵⁴ The trends in the slopes reflect differences in the keto group's sensitivity on different pigments (e.g., the slope is 10–20% less on Chl *a* (Figure 3b) and BPhe *a* (Figure 3c)). The lower correlations obtained on photosynthetic pigments relative to previous studies on

acetophenone (R^2 of 0.99)³⁶ and other carbonyl groups⁴² may be due to the inability of MD simulations to describe the more complex solvation structure around a large polyfunctional molecule, or to the possibility that the coordination environment around Mg could be solvent-dependent, implying that the pigments exist as slightly different complexes in different solvents.

The acetyl vibration was not as well resolved in many solvents as it is in the low-temperature spectra in Figure 2, making it impossible to systematically probe its frequency shifts in response to the solvent electric field. The ester vibration, in contrast, is well separated and peak frequencies were more reliably assigned. However, the 7c- and 10a-esters experience significantly different solvent fields in most of our simulations (see Table S2), while their vibrational bands overlap, resulting in a less precise description of their solvatochromism. Nevertheless, R^2 values around 0.6–0.8 were obtained by plotting the ester peak frequencies against the 10a-ester electric field, and the slopes [$0.46\text{ cm}^{-1}/(\text{MV}/\text{cm})$ for BChl *a*, $0.45\text{ cm}^{-1}/(\text{MV}/\text{cm})$ for Chl *a*] were approximately half of those for the 9-keto groups, consistent with the ca. 2-fold lower field sensitivity found in vibrational Stark spectroscopy (Table 1).

4. DISCUSSION

In the present study, we use vibrational Stark spectroscopy to probe electric fields and electric field differences on the L- and M-sides of the RC. Carbonyl vibrational probes are better suited for this purpose than electronic transitions for several reasons. First, the observed vibrational frequencies are not influenced by electronic coupling between the chromophores. Second, the use of localized vibrational reporter groups yields the projection of electric fields at a precise location because the orientation of $\Delta\vec{\mu}_{\text{C}=\text{O}}$ is known from the X-ray structure as it is parallel to $\text{C}=\text{O}$ bond axis. In particular, using the intrinsic carbonyl probes of the chromophores, which are part of the ET chain, is ideal because both BChl and BPhe have four independent reporter groups of electric field (9-keto, 2-acetyl and two ester groups). As shown above, the Stark tuning rate of the most relevant 9-keto and 2-acetyl carbonyl groups are found to be large, and the observed frequency shifts report on electric fields, including those due to hydrogen bonds.³⁶ Because there is a pseudo C_2 -symmetry axis between the L- and M-side in the RC, we can directly interpret differences in the vibrational frequencies of the chromophores in symmetry-related positions as differences in the projection of electric fields onto the reporter group. Fourth, as discussed in the following, a large body of data is available in the literature on each vibrational frequency in the RC. The vibrational Stark effect framework brings a different and quantitative perspective to the analysis of absolute shifts and differences on the L- and M-side chromophore environments.

Important symmetry-breaking amino acids (i.e., not conserved between the paralogous chains) in the immediate vicinity of the special pair, the bacteriopheophytins, and H_L and H_M , in particular those near to the carbonyl groups that we are using as probes, are illustrated in Figure 4. While there are significant differences in the vicinities of B_L and B_M , for example, Tyr M210 versus Phe L181, these do not directly interact with the carbonyl groups.^{2,43} A large body of literature is available on the measurement and assignment of the vibrational frequencies of the 9-keto and 2-acetyl groups of the BChls and BPhe in the RC from *Rb. sphaeroides*. In particular,

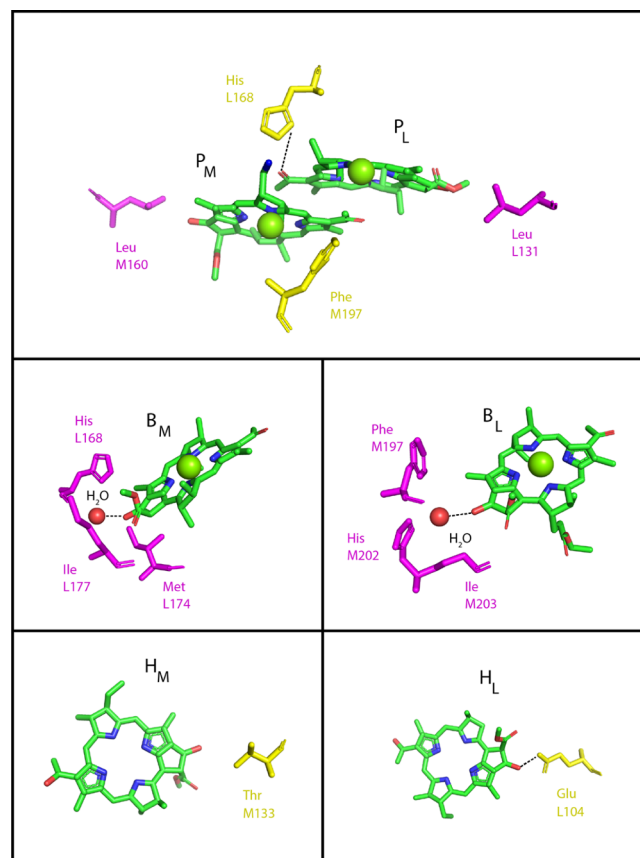


Figure 4. Amino acids that break the symmetry between the L- and M-branches in the vicinity of chromophores in *Rb. sphaeroides* RCs (pdb entry 2J8C). Symmetry-breaking amino acids are shown in yellow while nonsymmetry-breaking amino acids are shown in magenta. Note that the chromophore alignment is modified from the X-ray structure to better visualize the local environment of the 9-keto groups. For the special pair, the 2-acetyl group of P_L is hydrogen-bonded to His L168 with Phe M197 in the symmetry-related position at P_M . There are no symmetry-breaking amino acids hydrogen bonded to the B_M and B_L residues. For the bacteriopheophytins, protonated Glu L104 hydrogen bonds to the 9-keto group of H_L while the 9-keto group of H_M is not hydrogen bonded.

numerous studies focused on the assignment of hydrogen bonds to the 9-keto and 2-acetyl groups because they are part of the delocalized π -system and any change in H-bonding is expected to affect the redox properties of the chromophores and hence, ET rates.⁴⁴ Light-minus-dark FTIR difference spectroscopy, pioneered by Breton et al.^{21,45} allows for the assignment of the carbonyl frequencies of the chromophores in the part of the RC, where ET occurs (P_L , B_L , H_L , Q_A , and Q_B).^{5,21,45} Vibrational frequencies of the chromophores in the inactive M-branch (P_M , B_M , and H_M) cannot be assigned using this method. In contrast, resonance Raman techniques enable assignment of the carbonyl modes of all chromophores because the ground electronic absorption spectrum shows well-enough resolved bands for all chromophores at low temperature allowing for selective enhancement of vibrational modes of each individual chromophore.^{46,47}

Because we are interested in differences in electric fields at symmetry-related positions, we used the data obtained with Raman spectroscopy because we can directly compare differences in vibrational frequencies between the L- and M-side (Table 2). In the following, we will discuss differences in

Table 2. Vibrational Frequencies of the Chromophore Carbonyl Modes in Wild-Type RCs Assigned by Different Groups Using Resonance Raman Spectroscopy (*Rb. sphaeroides* in Black, *Rb. capsulatus* in Red). Differences in the Projection of the Electric Fields onto the Carbonyl Bonds ΔF_{L-M} in MV/cm between Pigments in L- and M-Branes Were Calculated from the Frequency Shifts and the Stark Tuning Rates Summarized in Table 1.

9-keto carbonyl					2-acetyl carbonyl				
P_L	P_M	Δ_{L-M}	ΔF_{L-M} (MV/cm)	Ref.	P_L	P_M	Δ_{L-M}	ΔF_{L-M} (MV/cm)	Ref.
1692	1684	+8	+2.6	46	1636	1660	-24	-10.4	46
1691	1679	+12	+3.9	50-51	1620	1653	-33	-14.3	50-51
1697	1678	+19	+6.1	52	1637	1660	-23	-10.0	53
B_L^a	B_M^a	Δ_{L-M}^a	ΔF_{L-M} (MV/cm)	Ref.	B_L^a	B_M^a	Δ_{L-M}^a	ΔF_{L-M} (MV/cm)	Ref.
1689	1685	$\pm 4^a$	± 1.3	46	1660	1663	$\pm 3^a$	± 1.3	46
1691	1687	$\pm 4^a$	± 1.3	22	1672	1669	$\pm 3^a$	± 1.3	52
1693	1689	$\pm 4^a$	± 1.3	52	1659	1663	$\pm 4^a$	± 1.7	53
1685(7)	1685(7)	$\pm 0.2^c$	$\pm (0.6)$	54	1662	1662	0	0	54
H_L	H_M	Δ_{L-M}	ΔF_{L-M} (MV/cm)	Ref.	H_L	H_M	Δ_{L-M}	ΔF_{L-M} (MV/cm)	Ref.
1678	1708	-30	-11.1	46	1633	1627	+6	+3.3	46
1678	1703	-25	-9.3	55	1633	1627	+6	+3.3	55
1683	1709 ^b	-26	-9.6	52	1635	1625	+10	+5.6	53
1686	1705	-19	-7.0	56					

^a L- and M-side not assigned

^b Shoulder at 1703 cm⁻¹

^c Both bands lie between 1685-1687 cm⁻¹

electric fields and hydrogen bonding between the pigments on the L- and M-side. Note that one drawback of Raman spectroscopy is the weak Raman intensity of the ester groups. Therefore, our analysis is limited to the 9-keto and 2-acetyl groups of the pigments. We also note that the 2-acetyl and ester carbonyls are on side chains that have conformational flexibility that could result in different projections of the protein field on $\Delta\vec{\mu}_{C=O}$; thus, we primarily focus on the 9-keto carbonyls which are fixed. As noted in Table 2, different investigators have obtained somewhat different values and while most data are available for *Rb. sphaeroides*, we include limited data for closely related *Rb. capsulatus* as well.

In considering what to emphasize, we begin with three important limitations. First, the acetyl groups of the chromophores are rotated out of the plane in several chromophores. This might affect the intrinsic Stark tuning rate and would not be captured by measurements in a frozen glass or solvatochromism in solution. Furthermore, because the measured fields are projections onto $\Delta\vec{\mu}$ differences in orientation of the carbonyl functionality of acetyl groups could affect the analysis. Second, some carbonyl groups are hydrogen bonded and this creates a local electrostatic field that shifts the carbonyl frequency. Within the resolution of the X-ray structures, all of these H-bonds appear to be normal H-bonds and are therefore expected to produce comparable shifts.³⁶ Third, the fields being reported are local projections sensed by the carbonyl probes. Because primary charge separation involves the creation of large electric dipoles from

neutrals, tens of Debye in magnitude, even small field differences can have a substantial effect on the energetics of charge separation. This is in contrast to typical changes in the dipole moment involved in chemical or enzymatic catalysis, where charge shifts over distances on the order of a bond length, at most a change of a Debye, and so larger fields are needed to affect activation free energies.^{48,49}

The crystal structure of *Rb. sphaeroides* reveals no hydrogen bonding partners for the 9-keto groups of P_L and P_M (the closest amino acids are leucine L131 and leucine M160 in the symmetry-related position). The modest differences in vibrational frequencies can therefore be attributed to differences in the electrostatic environment, between 8 and 19 cm⁻¹ implying $\Delta\vec{F}_{L-M} \approx (2.5-5.9)f$ MV/cm, a relatively minor difference. The 2-acetyl groups show a larger difference in frequency, between 23 and 33 cm⁻¹ due, at least in part, to a difference in hydrogen bonding because the 2-acetyl group of P_L is hydrogen bonded to His L168, while the symmetry-related Phe M197 does not form a hydrogen bond to P_M . A comprehensive study by Mattioli et al. investigated the changes in midpoint potentials of P associated with hydrogen bond changes at the carbonyls; the symmetry mutant in which His L168 was replaced by Phe shows that the 2-acetyl frequencies of P_L and P_M are identical, indicating a similar electrostatic environment (both at 1653 cm⁻¹).^{50,57} These results suggest that the global electrostatic asymmetry around P is small. The hydrogen bond between the 2-acetyl group of P_L and His L168 may contribute to the stabilization of the charge displacement

associated with excitation of P to P* as observed in electronic Stark spectra of P.⁵⁸

None of the carbonyl groups of the accessory BChls B_L and B_M are hydrogen-bonded. The observed differences in vibrational frequencies are all <4 cm⁻¹, indicating a very similar electrostatic environment for both B_L and B_M in the ground state; the difference in the projection of electric field is (1–2)f MV/cm at both the 9-keto and 2-acetyl group. For *Rb. capsulatus* RCs, the vibrational frequencies of the 9-keto groups differ by less than 2 cm⁻¹ and the frequencies of the 2-acetyl groups are identical.²² This indicates that electrostatic differences projected onto the keto groups of the accessory BChls in the electronic ground state are not of crucial importance for unidirectional ET. The absence of hydrogen bonds is reflected in vibrational frequencies between 1685 and 1690 cm⁻¹ for the 9-keto group and 1660 cm⁻¹ for the 2-acetyl group. By reference to Figure 3 and Table S1, these frequencies correspond to small electrostatic fields on an absolute basis and are consistent with a relatively nonpolar environment, comparable to that found in ether, for the carbonyl groups.

The 9-keto group of H_L is hydrogen-bonded to the protonated glutamic acid L104, while the symmetry-related threonine M133 is not hydrogen-bonded to H_M. H_L's 9-keto group is concomitantly shifted 20–30 cm⁻¹ to the red, suggesting a significant electrostatic field arising from this local hydrogen bonding interaction and a typical hydrogen bond shift. In *Rb. capsulatus*, the symmetry mutant where Glu L104 has been replaced with leucine still shows a difference of ~14 cm⁻¹ between the 9-keto groups, which would correspond to a difference in electric fields of ~5f MV/cm, suggesting that the difference in the electric field projected on the 9-keto carbonyl observed in *Rb. sphaeroides* reflects a combination of local hydrogen bonding and more distal interactions.⁵⁶ There are no hydrogen bonding partners for the 2-acetyl group of both H_L and H_M, and the difference in frequency is smaller, 6–10 cm⁻¹ ($\Delta\vec{F}_{L-M} \approx (3-5)f$ MV/cm), reflecting small electrostatic differences arising from the protein matrix.

The field-frequency curves reveal that the electric field experienced by B's 9-keto group in the *Rb. sphaeroides* RC is small on an absolute basis on both the L-branch (−7 MV/cm) and M-branch (−11 MV/cm)—comparable to the solvent ether, whereas H_M's 9-keto experiences a similarly small overall electric field (−6 MV/cm), the hydrogen-bonded H_L's electric field is large (−40 MV/cm), though assigning it an absolute value requires extrapolation beyond the domain delineated by the solvent series.

5. CONCLUSIONS

We have quantified differences in electric fields in symmetry-related positions between the active L- and the inactive M-side in the RC of the purple bacterium *Rb. sphaeroides* using the vibrational Stark effect. We used the intrinsic carbonyl groups of the pigments as the reporter of electric fields. The vibrational Stark effects of the carbonyls are large, most likely because of a large electronic contribution of the π -macrocycle to the Stark tuning rate. The overall differences in vibrational frequencies between the L- and M-side are very small for B_L versus B_M. Given the critical role of B_L in mediating primary charge separation, the negligible difference in the field projected on the 9-keto carbonyl group of B_L versus B_M suggests that this is not a primary determinant of bias toward the L-side. An important caveat that is intrinsic to our

approach is that we measure the specific projection of the protein electric field onto the C=O bond. Because we do not know *a priori* what the direction of the global field is, it could be that the 9-keto carbonyls of the monomeric bacteriochlorophylls are nearly orthogonal to the field. Thus, the strategy of using these intrinsic and essentially perfectly symmetry-related probes has this built-in limitation. One way around this will be to engineer probes such as aromatic nitrile-containing amino acids into the RC at symmetry-related positions using amber suppression.¹⁸ For example, in preliminary work, we have found the o-CN-phenylalanine can be incorporated close to H_L, and structural characterization demonstrates a single orientation for the −CN IR probe (J. Weaver and S.G. Boxer, to be published). This strategy should produce a more comprehensive mapping of electrostatic field differences on the L- and M-sides.

In contrast with the BChls, the difference in frequencies are as large as 30 cm⁻¹ for H_L versus H_M, where the larger shifts reflect the strong electrostatic fields arising from H-bonding interactions. Because of the large values of the difference dipoles, shifts of 30 cm⁻¹ correspond to a difference in the electric field of 10f MV/cm for the 9-keto mode and below 15f MV/cm for the 2-acetyl mode. While not large in comparison to the effects associated with strong short hydrogen bonds,^{25,36} a field difference of this magnitude could be energetically significant when considering the stabilization of long-range charge transfer, and in the present case, could be a significant determinant of the ~65:1 preference for electron transfer along the L-branch, which would require the primary intermediate (P⁺H_L[−]) to be ~2.5 kcal mol^{−1} more stable than the alternative (P⁺H_M[−]). The larger electrostatic field on H_L's 9-keto cannot directly explain the preference for L-branch ET because electrostatic stabilization of H_L[−] will depend on the field on all regions of H_L where the transferred charge can delocalize. Nevertheless, the order of magnitude of this measured field difference (10f MV/cm), the dipole associated with charge transfer (2–10 D), and the energetic preference (2.5 kcal mol^{−1}) are all roughly consistent by the equation $\Delta U = \Delta\vec{F} \cdot \Delta\vec{\mu}$ (note that 1 MV/cm \approx 0.048 kcal mol^{−1} D^{−1}).

In summary, the data in Table 2 are consistent with the possibility that H_L[−] can be stabilized over H_M[−] by a combination of a standard-strength hydrogen-bond (from Glu L104) and a global electric field effect that renders the environment surrounding H_L an effectively “more polar solvent” than the analogous region surrounding H_M. This hypothesis could be further examined by computationally examining the change in dipole on the 9-keto group of BPhe a upon one-electron reduction, to determine the energetic difference that would accompany the electrostatic field difference at this position. This study is an example of how new approaches, such as the vibrational Stark effect, can shed light on long-standing questions about charge transfer in reaction centers, and in protein biophysics more generally.

■ ASSOCIATED CONTENT

Supporting Information

The Supporting Information is available free of charge on the ACS Publications website at DOI: 10.1021/acs.jpcb.8b11458.

FTIR and Stark spectra of plant pigments; vibrational frequencies of isolated chromophores in different organic solvents; and MD parameters and calculated electric fields for chromophores (PDF)

AUTHOR INFORMATION

Corresponding Author

*E-mail: sboxer@stanford.edu.

ORCID

Steven G. Boxer: [0000-0001-9167-4286](https://orcid.org/0000-0001-9167-4286)

Present Addresses

[†]Late Stage Pharmaceutical Development, Genentech Inc., South San Francisco, California 94080, USA (M.S.).

[‡]Department of Chemistry, Johns Hopkins University, Remsen Hall Room 121, 3400 N. Charles Street, Baltimore, Maryland 21218, USA (S.D.F.).

Notes

The authors declare no competing financial interest.

ACKNOWLEDGMENTS

This paper is dedicated to the memory of Jacques Breton who pioneered the application of FTIR to understanding local interactions in the reaction center. M.S. was supported by a DFG Forschungsstipendium (Deutsche Forschungsgemeinschaft, Sa 2156/1-1). S.D.F. was supported by an NSF predoctoral fellowship program and a Stanford Bio-X interdisciplinary graduate fellowship. We greatly appreciate long-standing support for this work from the NSF Biophysics Program (MCB1408785).

REFERENCES

- Blankenship, R. E. *Molecular Mechanisms of Photosynthesis*; John Wiley & Sons, 2014.
- Ermler, U.; Fritzsch, G.; Buchanan, S. K.; Michel, H. Structure of the photosynthetic reaction centre from Rhodobacter sphaeroides at 2.65 Å resolution: cofactors and protein-cofactor interactions. *Structure* **1994**, *2*, 925–936.
- Deisenhofer, J.; Epp, O.; Miki, K.; Huber, R.; Michel, H. X-ray structure analysis of a membrane protein complex. *J. Mol. Biol.* **1984**, *180*, 385–398.
- Kirmaier, C.; Holten, D. Primary Photochemistry of Reaction Centers from the Photosynthetic Purple Bacteria. *Photosynth. Res.* **1987**, *13*, 225–260.
- Breton, J.; Boullais, C.; Burie, J.-R.; Nabedryk, E.; Mioskowski, C. Binding Sites of Quinones in Photosynthetic Bacterial Reaction Centers Investigated by Light-Induced FTIR Difference Spectroscopy: Assignment of the Interactions of Each Carbonyl of Q_a in Rhodobacter Sphaeroides Using Site-Specific ¹³C-Labeled Ubiquinone. *Biochemistry* **2002**, *33*, 14378–14386.
- Carter, B.; Boxer, S. G.; Holten, D.; Kirmaier, C. Trapping the P+BL-Initial Intermediate State of Charge Separation in Photosynthetic Reaction Centers from Rhodobacter capsulatus. *Biochemistry* **2009**, *48*, 2571–2573.
- Zhang, L. Y.; Friesner, R. A. Ab Initio Calculation of Electronic Coupling in the Photosynthetic Reaction Center. *Proc. Natl. Acad. Sci. U.S.A.* **1998**, *95*, 13603–13605.
- Steffen, M. A.; Lao, K.; Boxer, S. G. Dielectric Asymmetry in the Photosynthetic Reaction Center. *Science* **1994**, *264*, 810–816.
- Alden, R. G.; Parson, W. W.; Chu, Z. T.; Warshel, A. Calculations of Electrostatic Energies in Photosynthetic Reaction Centers. *J. Am. Chem. Soc.* **1995**, *117*, 12284–12298.
- Gunner, M. R.; Nicholls, A.; Honig, B. Electrostatic Potentials in Rhodopseudomonas viridis Reaction Centers: Implications for the Driving Force and Directionality of Electron Transfer. *J. Phys. Chem.* **1996**, *100*, 4277–4291.
- Kim, H.; Cho, M. Infrared Probes for Studying the Structure and Dynamics of Biomolecules. *Chem. Rev.* **2013**, *113*, 5817–5847.
- Waegelle, M. M.; Culik, R. M.; Gai, F. Site-Specific Spectroscopic Reporters of the Local Electric Field, Hydration, Structure, and Dynamics of Biomolecules. *J. Phys. Chem. Lett.* **2011**, *2*, 2598–2609.
- Fafarman, A. T.; Boxer, S. G. Nitrile Bonds as Infrared Probes of Electrostatics in Ribonuclease S. *J. Phys. Chem. B* **2010**, *114*, 13536–13544.
- Fafarman, A. T.; Webb, L. J.; Chuang, J. I.; Boxer, S. G. Site-Specific Conversion of Cysteine Thiols into Thiocyanate Creates an Ir Probe for Electric Fields in Proteins. *J. Am. Chem. Soc.* **2006**, *128*, 13356–13357.
- Jo, H.; Culik, R. M.; Korendovych, I. V.; DeGrado, W. F.; Gai, F. Selective Incorporation of Nitrile-Based Infrared Probes into Proteins Via Cysteine Alkylation. *Biochemistry* **2010**, *49*, 10354–10356.
- Fafarman, A. T. Quantitative Measurements of Electrostatic Fields in Proteins Using Vibrational Probes. Ph.D. Thesis, Stanford University, 2010.
- Chuang, J. Understanding Unidirectional Electron Transfer in the Photosynthetic Reaction Center Using Protein Engineering. Ph.D. Thesis, Stanford University, 2007.
- Weaver, J. B.; Boxer, S. G. Genetic Code Expansion in Rhodobacter Sphaeroides to Incorporate Noncanonical Amino Acids into Photosynthetic Reaction Centers. *ACS Synth. Biol.* **2018**, *7*, 1618–1628.
- Konar, A.; Sechrist, R.; Song, Y.; Policht, V. R.; Laible, P. D.; Bocian, D. F.; Holten, D.; Kirmaier, C.; Ogilvie, J. P. Electronic Interactions in the Bacterial Reaction Center Revealed by Two-Color 2d Electronic Spectroscopy. *J. Phys. Chem. Lett.* **2018**, *9*, 5219–5225.
- Ma, F.; Romero, E.; Jones, M. R.; Novoderezhkin, V. I.; van Grondelle, R. Vibronic Coherence in the Charge Separation Process of the Rhodobacter Sphaeroides Reaction Center. *J. Phys. Chem. Lett.* **2018**, *9*, 1827–1832.
- Mantele, W. G.; Wollenweber, A. M.; Nabedryk, E.; Breton, J. Infrared Spectroelectrochemistry of Bacteriochlorophylls and Bacteriopheophytins: Implications for the Binding of the Pigments in the Reaction Center from Photosynthetic Bacteria. *Proc. Natl. Acad. Sci. U.S.A.* **1988**, *85*, 8468–8472.
- Kirmaier, C.; Laible, P. D.; Czarnecki, K.; Hata, A. N.; Hanson, D. K.; Bocian, D. F.; Holten, D. Comparison of M-Side Electron Transfer in Rb.sphaeroides and Rb.capsulatus Reaction Centers. *J. Phys. Chem. B* **2002**, *106*, 1799–1808.
- Mattioli, T. A.; Williams, J. C.; Allen, J. P.; Robert, B. Changes in primary donor hydrogen-bonding interactions in mutant reaction centers from Rhodobacter sphaeroides: identification of the vibrational frequencies of all the conjugated carbonyl groups. *Biochemistry* **2002**, *33*, 1636–1643.
- Suydam, I. T.; Boxer, S. G. Vibrational Stark Effects Calibrate the Sensitivity of Vibrational Probes for Electric Fields in Proteins. *Biochemistry* **2003**, *42*, 12050–12055.
- Fried, S. D.; Boxer, S. G. Measuring Electric Fields and Noncovalent Interactions Using the Vibrational Stark Effect. *Acc. Chem. Res.* **2015**, *48*, 998–1006.
- Laible, P. D.; Kirmaier, C.; Udawatte, C. S. M.; Hofman, S. J.; Holten, D.; Hanson, D. K. Quinone Reduction via Secondary B-Branch Electron Transfer in Mutant Bacterial Reaction Centers. *Biochemistry* **2003**, *42*, 1718–1730.
- Scheer, H. *Chlorophylls*; CRC Press LLC, 1991.
- Omata, T.; Murata, N. Preparation of Chlorophyll a, Chlorophyll B and Bacteriochlorophyll a by Column Chromatography with Deae-Sepharose Cl-6b and Sepharose Cl-6b. *Plant Cell Physiol.* **1983**, *24*, 1093–1100.
- Andrews, S. S.; Boxer, S. G. A Liquid Nitrogen Immersion Cryostat for Optical Measurements. *Rev. Sci. Instrum.* **2000**, *71*, 3567–3569.
- Andrews, S. S.; Boxer, S. G. Vibrational Stark Effects of Nitriles I. Methods and Experimental Results. *J. Phys. Chem. A* **2000**, *104*, 11853–11863.
- Bublitz, G. U.; Boxer, S. G. Stark Spectroscopy: Applications in Chemistry, Biology, and Materials Science. *Annu. Rev. Phys. Chem.* **1997**, *48*, 213–242.

- (32) *Spectfit*, Version 2.0, <http://www.smoldyn.org/andrews/software.html>.
- (33) Zhang, L.; Silva, D.-A.; Yan, Y.; Huang, X. Force Field Development for Cofactors in the Photosystem II. *J. Comput. Chem.* **2012**, *33*, 1969–1980.
- (34) Ceccarelli, M.; Procacci, P.; Marchi, M. An ab initio force field for the cofactors of bacterial photosynthesis. *J. Comput. Chem.* **2002**, *24*, 129–142.
- (35) Caleman, C.; van Maaren, P. J.; Hong, M.; Hub, J. S.; Costa, L. T.; van der Spoel, D. Force Field Benchmark of Organic Liquids: Density, Enthalpy of Vaporization, Heat Capacities, Surface Tension, Isothermal Compressibility, Volumetric Expansion Coefficient, and Dielectric Constant. *J. Chem. Theory Comput.* **2011**, *8*, 61–74.
- (36) Fried, S. D.; Bagchi, S.; Boxer, S. G. Measuring Electrostatic Fields in Both Hydrogen-Bonding and Non-Hydrogen-Bonding Environments Using Carbonyl Vibrational Probes. *J. Am. Chem. Soc.* **2013**, *135*, 11181–11192.
- (37) Blankenship, R. E.; Madigan, M. T.; Bauer, C. E. *Anoxygenic Photosynthetic Bacteria*; Springer Science & Business Media, 2006; Vol. 2.
- (38) Saggau, M.; Levinson, N. M.; Boxer, S. G. Experimental Quantification of Electrostatics in X-H \cdots π Hydrogen Bonds. *J. Am. Chem. Soc.* **2012**, *134*, 18986–18997.
- (39) Park, E. S.; Boxer, S. G. Origins of the Sensitivity of Molecular Vibrations to Electric Fields: Carbonyl and Nitrosyl Stretches in Model Compounds and Proteins. *J. Phys. Chem. B* **2002**, *106*, 5800–5806.
- (40) Breton, J.; Burie, J.-R.; Berthomieu, C.; Berger, G.; Nabedryk, E. The Binding Sites of Quinones in Photosynthetic Bacterial Reaction Centers Investigated by Light-Induced FTIR Difference Spectroscopy: Assignment of the QA Vibrations in Rhodobacter sphaeroides Using ^{18}O - or ^{13}C -Labeled Ubiquinones and Vitamin K1. *Biochemistry* **2002**, *33*, 4953–4965.
- (41) Bellamy, L. J.; Williams, R. L. Infra-red spectra and solvent effects. Part 2.-Carbonyl absorptions. *Trans. Faraday Soc.* **1959**, *55*, 14–18.
- (42) Schneider, S. H.; Kratochvil, H. T.; Zanni, M. T.; Boxer, S. G. Solvent-Independent Anharmonicity for Carbonyl Oscillators. *J. Phys. Chem. B* **2017**, *121*, 2331–2338.
- (43) Koepke, J.; Krammer, E.-M.; Klingen, A. R.; Sebban, P.; Ullmann, G. M.; Fritzsch, G. Ph Modulates the Quinone Position in the Photosynthetic Reaction Center from Rhodobacter Sphaeroides in the Neutral and Charge Separated States. *J. Mol. Biol.* **2007**, *371*, 396–409.
- (44) Heller, B.; Holten, D.; Kirmaier, C. Control of electron transfer between the L- and M-sides of photosynthetic reaction centers. *Science* **1995**, *269*, 940–945.
- (45) Breton, J.; Bibikova, M.; Oesterhelt, D.; Nabedryk, E. Conformational Heterogeneity of the Bacteriopheophytin Electron Acceptor HA in Reaction Centers from Rhodopseudomonas viridis Revealed by Fourier Transform Infrared Spectroscopy and Site-Directed Mutagenesis. *Biochemistry* **1999**, *38*, 11541–11552.
- (46) Robert, B. Resonance Raman Studies of Bacterial Reaction Centers. *Biochim. Biophys. Acta* **1990**, *1017*, 99–111.
- (47) Frolov, D.; Gall, A.; Lutz, M.; Robert, B. Structural Asymmetry of Bacterial Reaction Centers: A Qy Resonant Raman Study of the Monomer Bacteriochlorophylls. *J. Phys. Chem. A* **2002**, *106*, 3605–3613.
- (48) Fried, S. D.; Bagchi, S.; Boxer, S. G. Extreme Electric Fields Power Catalysis in the Active Site of Ketosteroid Isomerase. *Science* **2014**, *346*, 1510.
- (49) Fried, S. D.; Boxer, S. G. Electric Fields and Enzyme Catalysis. *Annu. Rev. Biochem.* **2017**, *86*, 387–415.
- (50) Mattioli, T. A.; Lin, X.; Allen, J. P.; Williams, J. C. Correlation between Multiple Hydrogen Bonding and Alteration of the Oxidation Potential of the Bacteriochlorophyll Dimer of Reaction Centers from Rhodobacter Sphaeroides. *Biochemistry* **2002**, *34*, 6142–6152.
- (51) Mattioli, T. A.; Hoffmann, A.; Robert, B.; Schrader, B.; Lutz, M. Primary Donor Structure and Interactions in Bacterial Reaction Centers from near-Infrared Fourier Transform Resonance Raman Spectroscopy. *Biochemistry* **2002**, *30*, 4648–4654.
- (52) Palaniappan, V.; Martin, P. C.; Chynwat, V.; Frank, H. A.; Bocian, D. F. Comprehensive Resonance Raman Study of Photosynthetic Reaction Centers from Rhodobacter Sphaeroides. Implications for Pigment Structure and Pigment-Protein Interactions. *J. Am. Chem. Soc.* **1993**, *115*, 12035–12049.
- (53) Robert, B.; Lutz, M. Proteic Events Following Charge Separation in the Bacterial Reaction Center: Resonance Raman Spectroscopy. *Biochemistry* **2002**, *27*, 5108–5114.
- (54) Chen, L.; Kirmaier, C.; Holten, D.; Bocian, D. F. Resonance Raman Characterization of Rhodobacter Capsulatus Reaction Centers with Lysine Mutations near the Accessory Bacteriochlorophylls. *Photosynth. Res.* **2005**, *83*, 35–43.
- (55) Ivancich, A.; Lutz, M.; Mattioli, T. A. Temperature-Dependent Behavior of Bacteriochlorophyll and Bacteriopheophytin in the Photosynthetic Reaction Center from Rhodobacter sphaeroides. *Biochemistry* **1997**, *36*, 3242–3253.
- (56) Palaniappan, V.; Bocian, D. F. Resonance Raman Spectroscopic Evidence for Dielectric Asymmetry in Bacterial Photosynthetic Reaction Centers. *J. Am. Chem. Soc.* **1995**, *117*, 3647–3648.
- (57) Hughes, J. M.; Hutter, M. C.; Reimers, J. R.; Hush, N. S. Modeling the Bacterial Photosynthetic Reaction Center. 4. The Structural, Electrochemical, and Hydrogen-Bonding Properties of 22 Mutants of Rhodobacter sphaeroides. *J. Am. Chem. Soc.* **2001**, *123*, 8550–8563.
- (58) Moore, L. J.; Zhou, H.; Boxer, S. G. Excited-State Electronic Asymmetry of the Special Pair in Photosynthetic Reaction Center Mutants: Absorption and Stark Spectroscopy. *Biochemistry* **1999**, *38*, 11949–11960.

Supporting Information for
Local and Global Electric Field Asymmetry in
Photosynthetic Reaction Centers

Miguel Sagu[†], Stephen D. Fried[‡], and Steven G. Boxer^{*}

Department of Chemistry, Stanford University, Stanford, CA 94305-5080, USA

* To whom correspondence should be addressed: sboxer@stanford.edu

† Current address: Late Stage Pharmaceutical Development, Genentech Inc., South San Francisco, California 94080, USA

‡ Current address: Department of Chemistry, Johns Hopkins University, Remsen Hall Room 121, 3400 N. Charles Street, Baltimore, Md. 21218

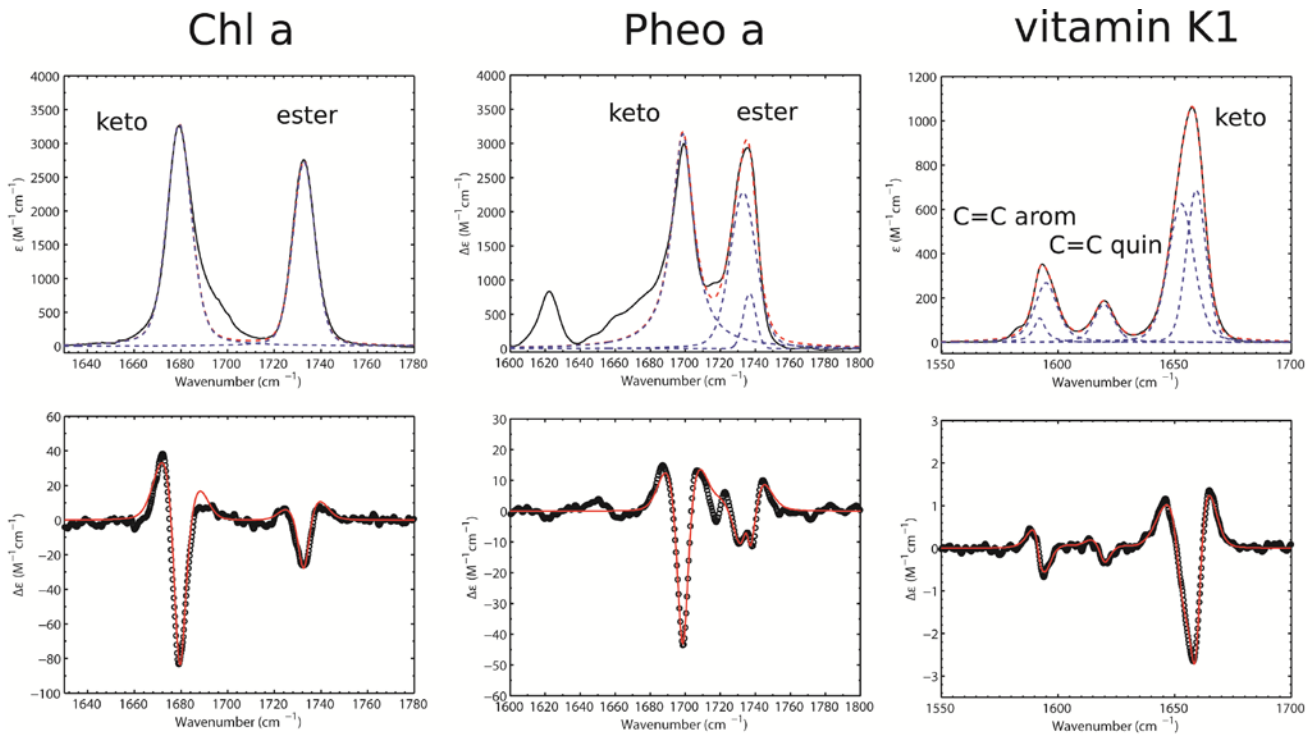


Figure S1 FTIR spectra in the carbonyl region (upper) and vibrational Stark spectra (lower) of photosynthetic chromophores at $T = 77$ K. 5 mM Chl *a* in 2-methyl-THF; 4.4 mM Phe *a* in 2-methyl-THF; 5 mM vitamin K1 in DCM/DCE. Vibrational Stark spectra are overlaid with best fits shown in red giving $|\Delta\bar{\mu}| \cdot f$ (see Table 1). Stark spectra are scaled to an external field of 1 MV/cm. ($\tilde{\nu}_{keto1} = 1659$ cm $^{-1}$, $\varepsilon_{\max} = 690$ M $^{-1}$ cm $^{-1}$; $\tilde{\nu}_{keto2} = 1653$ cm $^{-1}$, $\varepsilon_{\max} = 630$ M $^{-1}$ cm $^{-1}$; $\tilde{\nu}_{C=C-quin} = 1620$ cm $^{-1}$, $\varepsilon_{\max} = 170$ M $^{-1}$ cm $^{-1}$; $\tilde{\nu}_{C=C-arom} = 1595$ cm $^{-1}$, $\varepsilon_{\max} = 270$ M $^{-1}$ cm $^{-1}$; $\tilde{\nu}_{C=C-arom-sideband} = 1592$ cm $^{-1}$, $\varepsilon_{\max} = 110$ M $^{-1}$ cm $^{-1}$).

Table S1. Measured vibrational frequencies in cm^{-1} of the chromophores dissolved in various solvents. Note that BChl a and Chl a have 6 equivalents of pyridine added to keep them monomeric.

	BChl a			Chl a			BPhe a		
	ester	9-keto	acetyl	ester	9-keto	ester	9-keto	acetyl	
cyclohexane	1737.6	1698.4	1652.8	1741.2	1705.4	-	1712	1674	
Et ₂ O	1740	1692	1661	1740.7	1701.2	-	1708	1674	
THF	1737.6	1686	1653.8	1738	1695.3	-	1701	1669	
pyridine	1732.6	1675	1665	-	-	-	-	-	
ACN	1734.1	1678	1669	1735	1684.6	1733	1691	1666	
CHCl ₃	1730.4	1676	1661	1731	1679.1	1736	1698	1668	
DCM	1732.8	1674	1661	1733.4	1682.9	1737	1695	1670	
DMSO	1730.2	1668	1647	1732.3	1681	-	-	-	

Table S2. Calculated electric fields for vibrations of pigments dissolved in various solvents. Solvent fields reported as the average over the trajectory along with correlation-adjusted error (all in units of MV/cm). Standard deviations for each electric field entry are given as well (also in units of MV/cm). Abbreviations: CXH, cyclohexane; THF, tetrahydrofuran; DMF, dimethyl formamide; DMSO, dimethyl sulfoxide; DCM, dichloromethane; ACN, acetonitrile.

Chlorophyll

	9-keto			10a-ester			7c-ester		
	field	error	std. dev	field	error	std. dev	field	error	std. dev
CXH	-0.012434	0.023656	0.72541	0.075310	0.027132	0.70143	0.032271	0.062061	0.71385
ether	-11.818	0.39350	5.0922	-5.4610	0.34158	5.3904	-7.0494	0.78493	6.7588
THF	-16.580	0.26158	6.4229	-10.084	0.59645	7.0090	-11.644	0.31779	7.6801
pyridine	-21.362	0.49583	7.9482	-15.284	0.49193	9.2073	-17.616	0.56169	9.4654
acetone	-22.868	0.57787	8.3278	-12.547	0.54200	8.9251	-18.338	1.3510	10.084
DMF	-28.724	0.38922	8.6746	-17.273	1.1156	9.6087	-22.279	0.71904	10.537
DMSO	-27.285	1.0229	8.8723	-17.997	0.93743	9.8659	-20.856	0.62347	10.534
chloroform	-28.852	0.72160	13.438	-21.072	0.70419	13.608	-26.855	0.65203	13.062
DCM	-27.041	0.39646	12.350	-20.774	0.43520	12.906	-26.678	1.3158	12.822
acetonitrile	-24.712	0.098353	9.8358	-19.640	0.38013	10.762	-21.354	0.90245	11.142

Pheophytin

	9-keto			10a-ester			7c-ester		
	field	error	std. dev	field	error	std. dev	field	error	std. dev
CXH	0.047606	0.025706	0.71109	0.034830	0.033795	0.62259	0.090113	0.039419	0.72088
ether	-6.4665	0.33002	5.8862	-1.7574	0.40197	5.1855	-6.7318	0.49002	6.3743
THF	-12.832	0.20629	6.7143	-4.3022	0.44078	6.9236	-12.439	0.65038	8.2837
Pyridine	-20.898	0.32508	8.4505	-7.9185	0.86906	8.9438	-18.562	0.80535	9.6327
DMSO	-20.434	0.53520	10.084	-20.093	2.5480	11.855	-17.036	1.1437	11.874
chloroform	-29.231	0.64589	13.309	-13.731	1.5653	13.488	-20.098	1.5151	14.004
DCM	-26.710	0.51875	12.404	-18.621	1.1359	13.256	-22.132	1.6584	13.734

Bacteriochlorophyll

	9-keto			10a-ester			7c-ester			acetyl		
	field	error	std. dev	field	error	std. dev	field	error	std. dev	field	error	std. dev
CXH	0.054013	0.022260	0.69875	0.073631	0.048481	0.67948	-0.007154	0.022105	0.69095	0.055382	0.037273	0.74923
ether	-10.113	0.84137	7.1605	-5.9446	0.21272	6.0914	-6.7980	0.60884	6.6941	-12.368	0.82158	7.9643
THF	-12.363	0.89569	10.427	-8.5045	0.95322	9.1485	-11.519	0.43789	8.1643	-19.239	0.90590	12.899
pyridine	-17.049	1.9349	16.569	-10.148	1.4831	14.231	-14.761	1.2551	12.730	-23.137	1.5836	16.180
acetone	-18.999	1.4787	15.030	-10.382	1.3241	13.699	-14.072	1.4591	14.119	-20.820	2.0771	20.736
ACN	-23.520	0.44058	12.601	-19.827	0.36622	12.152	-18.348	1.1800	15.513	-29.172	0.33759	13.199
DMSO	-26.088	2.9826	17.885	-19.640	2.3330	13.844	-11.327	1.1909	19.446	-30.964	4.3024	22.652
CHCl₃	-22.038	2.7595	24.086	-16.197	1.0916	18.154	-19.557	1.8361	17.880	-22.224	0.92275	15.643
DCM	-24.931	1.8336	17.239	-19.665	1.1948	15.125	-23.876	1.7767	18.048	-22.875	1.9388	16.199

Bacteriopheophytin

	9-keto			10a-ester			7c-ester			acetyl		
	field	mean	std. dev	field	mean	std. dev	field	mean	std. dev	field	mean	std. dev
CXH	0.015509	0.018469	0.66740	0.036457	0.013899	0.66987	-0.03076	0.017604	0.65336	-0.05899	0.025168	0.70917
ether	-7.3524	0.43306	5.3846	-5.7188	0.71410	5.9331	-6.2979	1.0797	6.8569	-13.996	0.19008	7.1971
THF	-11.429	0.11398	6.8194	-10.004	0.50608	7.7609	-9.6155	0.61233	8.2505	-22.816	0.28441	9.0821
pyridine	-21.772	0.78459	8.7748	-12.399	0.89186	9.2820	-14.945	1.1118	10.470	-26.907	0.73261	10.229
ACN	-21.191	0.33321	10.192	-19.638	0.56134	11.132	-18.530	1.7515	11.383	-30.103	0.15866	10.856
DMSO	-21.179	0.31720	9.7194	-22.270	1.1183	10.753	-18.727	1.5534	11.693	-43.764	0.78170	12.168
CHCl₃	-26.903	0.43056	13.582	-18.949	2.4155	14.421	-22.254	1.1588	13.977	-22.497	0.73714	12.591
DCM	-24.642	0.93726	12.710	-21.280	0.70513	13.121	-21.582	0.72130	12.767	-25.124	0.16564	11.438

Parameters for Bacteriochlorophyll (BCL) and Bacteriopheophytin (BPH).

Additional lines to the files *cofactors.hdb* and *cofactors.rtp* from Zhang's *amber03.ff* (GROMACS format). For digital versions, please e-mail Stephen Fried (sdfried@gmail.com).

Added to cofactors.hdb

BCL	37				
3	4	H7B	C7B	C6B	C3B
3	4	HMB	CMB	C2B	C1B
1	1	HHB	CHB	C1B	C4A
1	1	HHC	CHC	C4B	C1C
3	4	H5C	C5C	C2CX	C1C
3	4	HBC	CBC	CAC	C3CX
2	6	HAC	CAC	CBC	C3CX
1	5	H2CX	C2CX	C1C	C3CX C5C
1	5	H3CX	C3CX	C4C	C2CX CAC
1	1	HHD	CHD	C4C	C1D
3	4	HMD	CMD	C2D	C1D
1	5	HBD	CBD	CHA	CAD CGD
3	4	HED	CED	O2D	CGD
1	5	H3A	C3A	C4A	C2A CMA
3	4	HMA	CMA	C3A	C2A
1	5	H2A	C2A	C1A	C3A CAA
2	6	HAA	CAA	C2A	CBA
2	6	HBA	CBA	CGA	CAA
2	6	H1	C1	O2A	C2
1	1	H2	C2	C1	C3
3	4	H4	C4	C3	C2
2	6	H5	C5	C3	C6
2	6	H6	C6	C5	C7
2	6	H7	C7	C6	C8
1	5	H8	C8	C7	C9 C10
3	4	H9	C9	C8	C7
2	6	H10	C10	C8	C11
2	6	H11	C11	C10	C12
2	6	H12	C12	C11	C13
1	5	H13	C13	C12	C14 C15
3	4	H14	C14	C13	C12
2	6	H15	C15	C13	C16
2	6	H16	C16	C15	C17
2	6	H17	C17	C16	C18
1	5	H18	C18	C17	C19 C20
3	4	H19	C19	C18	C17
3	4	H20	C20	C18	C17
BPH	39				
3	4	H7B	C7B	C6B	C3B
3	4	HMB	CMB	C2B	C1B
1	1	HHB	CHB	C1B	C4A
1	1	HHC	CHC	C4B	C1C
3	4	H5C	C5C	C2CX	C1C
3	4	HBC	CBC	CAC	C3CX
2	6	HAC	CAC	CBC	C3CX
1	5	H2CX	C2CX	C1C	C3CX C5C
1	5	H3CX	C3CX	C4C	C2CX CAC
1	1	HHD	CHD	C4C	C1D
3	4	HMD	CMD	C2D	C1D
1	5	HBD	CBD	CHA	CAD CGD

3	4	HED	CED	O2D	CGD	
1	5	H3A	C3A	C4A	C2A	CMA
3	4	HMA	CMA	C3A	C2A	
1	5	H2A	C2A	C1A	C3A	CAA
2	6	HAA	CAA	C2A	CBA	
2	6	HBA	CBA	CGA	CAA	
2	6	H1	C1	O2A	C2	
1	1	H2	C2	C1	C3	
3	4	H4	C4	C3	C2	
2	6	H5	C5	C3	C6	
2	6	H6	C6	C5	C7	
2	6	H7	C7	C6	C8	
1	5	H8	C8	C7	C9	C10
3	4	H9	C9	C8	C7	
2	6	H10	C10	C8	C11	
2	6	H11	C11	C10	C12	
2	6	H12	C12	C11	C13	
1	5	H13	C13	C12	C14	C15
3	4	H14	C14	C13	C12	
2	6	H15	C15	C13	C16	
2	6	H16	C16	C15	C17	
2	6	H17	C17	C16	C18	
1	5	H18	C18	C17	C19	C20
3	4	H19	C19	C18	C17	
3	4	H20	C20	C18	C17	
1	1	HB	NB	C1B	C4B	
1	1	HD	ND	C1D	C4D	

Added to cofactors.rtp

[BCL]				
[atoms]				
MG	mgc	1.140797	1	
CHA	csb	0.073563	2	
CHB	cab	-0.530666	3	
CHC	cab	-0.293706	4	
CHD	cab	-0.381654	5	
NA	ns	-0.401782	6	
C1A	ccs	-0.027935	7	
C2A	ct1	-0.100818	8	
C3A	ct1	0.259931	9	
C4A	ccs	0.273045	10	
CMA	ct3	-0.347802	11	
CAA	ct2	-0.066561	12	
CBA	ct2	-0.370595	13	
CGA	c2a	0.722546	14	
O1A	o2c	-0.577588	15	
O2A	o1c	-0.390978	16	
NB	nmh	-0.522883	17	
C1B	crb	0.290613	18	
C2B	cbb	0.056235	19	
C3B	cbb	-0.059508	20	
C4B	cnb	0.201631	21	
CMB	ct3	-0.196671	22	
C6B	c2e	0.6950	23	
C7B	ct3	-0.3920	24	
NC	ns	-0.500171	25	
C1C	ccs	0.173876	26	
C2CX	ct1	0.063127	27	

C3CX	ct1	-0.155844	28
C4C	ccs	0.313793	29
C5C	ct3	-0.242247	30
CAC	ct2	0.190617	31
CBC	ct3	-0.128605	32
ND	nmh	-0.496512	33
C1D	cpb	0.199807	34
C2D	cbb	0.067465	35
C3D	cbb	-0.256041	36
C4D	cqb	0.145335	37
CMD	ct3	-0.257732	38
CAD	c2k	0.711103	39
OBD	o2c	-0.57472	40
CBD	ct1	-0.635795	41
CGD	c2a	0.907866	42
O1D	o2c	-0.603021	43
O2D	o1c	-0.381813	44
CED	ct3	0.011315	45
C1	ct2	0.183261	46
C2	cqq	-0.404524	47
C3	cq2	0.231494	48
C4	ct3	-0.171786	49
C5	ct2	-0.329157	50
C6	ct2	0.107607	51
C7	ct2	-0.097062	52
C8	ct1	0.223668	53
C9	ct3	-0.306973	54
C10	ct2	-0.096255	55
C11	ct2	0.050839	56
C12	ct2	-0.149838	57
C13	ct1	0.277566	58
C14	ct3	-0.306597	59
C15	ct2	-0.133326	60
C16	ct2	0.063751	61
C17	ct2	-0.174116	62
C18	ct1	0.431195	63
C19	ct3	-0.351586	64
C20	ct3	-0.351586	65
HHB	HA	0.18194	66
HHC	HA	0.147981	67
HHD	HA	0.220211	68
H2A	HC	0.11891	69
H3A	HC	0.009865	70
HMA1	HC	0.088879	71
HMA2	HC	0.088879	72
HMA3	HC	0.088879	73
HAA1	HC	0.074129	74
HAA2	HC	0.074129	75
HBA1	HC	0.123685	76
HBA2	HC	0.123685	77
HMB1	HC	0.069103	78
HMB2	HC	0.069103	79
HMB3	HC	0.069103	80
OB	o2c	-0.5370	81
H7B1	HC	0.075196	82
H7B2	HC	0.075196	83
H5C1	HC	0.07984	84
H5C2	HC	0.07984	85
H5C3	HC	0.07984	86

HAC1	HC	-0.010598	87
HAC2	HC	-0.010598	88
HBC1	HC	0.029396	89
HBC2	HC	0.029396	90
HBC3	HC	0.029396	91
HMD1	HC	0.084447	92
HMD2	HC	0.084447	93
HMD3	HC	0.084447	94
HBD	HC	0.195581	95
HED1	HC	0.069208	96
HED2	HC	0.069208	97
HED3	HC	0.069208	98
H11	HC	0.067685	99
H12	HC	0.067685	100
H2	HA	0.189077	101
H41	HC	0.059658	102
H42	HC	0.059658	103
H43	HC	0.059658	104
H51	HC	0.095476	105
H52	HC	0.095476	106
H61	HC	0.000653	107
H62	HC	0.000653	108
H71	HC	0.012281	109
H72	HC	0.012281	110
H8	HC	-0.018459	111
H91	HC	0.063458	112
H92	HC	0.063458	113
H93	HC	0.063458	114
H101	HC	0.017558	115
H102	HC	0.017558	116
H111	HC	0.003086	117
H112	HC	0.003086	118
H121	HC	0.028404	119
H122	HC	0.028404	120
H13	HC	-0.028733	121
H141	HC	0.059372	122
H142	HC	0.059372	123
H143	HC	0.059372	124
H151	HC	0.028933	125
H152	HC	0.028933	126
H161	HC	-0.009013	127
H162	HC	-0.009013	128
H171	HC	0.028341	129
H172	HC	0.028341	130
H18	HC	-0.060142	131
H191	HC	0.06933	132
H192	HC	0.06933	133
H193	HC	0.06933	134
H201	HC	0.06933	135
H202	HC	0.06933	136
H203	HC	0.06933	137
H2CX	HC	0.063127	138
H3CX	HC	-0.155844	139
H7B3	HC	0.075196	140

[bonds]
 C1B C2B
 C2B C3B
 C3B C4B

C4B	NB
NB	C1B
C2B	CMB
C3B	C6B
C6B	OB
C6B	C7B
C4B	CHC
CHC	C1C
C1C	C2CX
C2CX	H2CX
C2CX	C3CX
C3CX	H3CX
C3CX	C4C
C4C	NC
NC	C1C
C2CX	C5C
C3CX	CAC
CAC	CBC
C4C	CHD
CHD	C1D
C1D	C2D
C2D	C3D
C3D	C4D
C4D	ND
ND	C1D
C2D	CMD
C3D	CAD
CAD	CBD
CBD	CHA
CHA	C4D
CAD	OBD
CBD	CGD
CGD	O1D
CGD	O2D
O2D	CED
CHA	C1A
C1A	C2A
C2A	C3A
C3A	C4A
C4A	NA
NA	C1A
C4A	CHB
CHB	C1B
C3A	CMA
C2A	CAA
CAA	CBA
CBA	CGA
CGA	O1A
CGA	O2A
O2A	C1
C1	C2
C2	C3
C3	C4
C3	C5
C5	C6
C6	C7
C7	C8
C8	C9
C8	C10

C10 C11
C11 C12
C12 C13
C13 C14
C13 C15
C15 C16
C16 C17
C17 C18
C18 C19
C18 C20
CHB HHB
CHC HHC
CHD HHD
C2A H2A
C3A H3A
CMA HMA1
CMA HMA2
CMA HMA3
CAA HAA1
CAA HAA2
CBA HBA1
CBA HBA2
NB MG
CMB HMB1
CMB HMB2
CMB HMB3
C7B H7B1
C7B H7B2
C7B H7B3
C5C H5C1
C5C H5C2
C5C H5C3
CAC HAC1
CAC HAC2
CBC HBC1
CBC HBC2
CBC HBC3
ND MG
CMD HMD1
CMD HMD2
CMD HMD3
CBD HBD
CED HED1
CED HED2
CED HED3
C1 H11
C1 H12
C2 H2
C4 H41
C4 H42
C4 H43
C5 H51
C5 H52
C6 H61
C6 H62
C7 H71
C7 H72
C8 H8
C9 H91

```

C9  H92
C9  H93
C10 H101
C10 H102
C11 H111
C11 H112
C12 H121
C12 H122
C13 H13
C14 H141
C14 H142
C14 H143
C15 H151
C15 H152
C16 H161
C16 H162
C17 H171
C17 H172
C18 H18
C19 H191
C19 H192
C19 H193
C20 H201
C20 H202
C20 H203
MG  NC
MG  NA

```

```

[ angles ]
;   i       j       k           th0      cth
NA     MG     NC      176.1    418.400
NB     MG     ND      178.9    418.400

```

```

[ impropers ]
C3     C1     C2     H2
C2     C5     C3     C4
O2A    CBA    CGA    O1A
C2A    CHA    C1A    NA
C3A    CHB    C4A    NA
C1B    C4A    CHB    HHB
C4B    C2B    C3B    C6B
C3B    CHC    C4B    NB
C2B    CHB    C1B    NB
CMB    C3B    C2B    C1B
CBD    C4D    CHA    C1A
CBD    O2D    CGD    O1D
CBD    C3D    CAD    OBD
CAD    C4D    C3D    C2D
C3D    CHA    C4D    ND
C2D    CHD    C1D    ND
CMD    C1D    C2D    C3D
C1D    C4C    CHD    HHD
C3CX   CHD    C4C    NC
CAC    C2CX   C3CX   C4C
C2CX   CHC    C1C    NC
C5C    C1C    C2CX   C3CX
C1C    C4B    CHC    HHC

```

```

[ BPH ]
[ atoms ]
  C19      ct3      -0.35398      1
  H191     HC       0.07347      2
  H192     HC       0.07347      3
  H193     HC       0.07347      4
  C18      ct1      0.38934      5
  C20      ct3      -0.35398      6
  H201     HC       0.07347      7
  H202     HC       0.07347      8
  H203     HC       0.07347      9
  H18      HC      -0.04653     10
  C17      ct2      -0.15263     11
  H171     HC       0.03273     12
  H172     HC       0.03273     13
  C16      ct2      -0.00189     14
  H161     HC       0.00974     15
  H162     HC       0.00974     16
  C15      ct2      -0.17051     17
  H151     HC       0.03664     18
  H152     HC       0.03664     19
  C13      ct1      0.38169     20
  C14      ct3      -0.33615     21
  H141     HC       0.07019     22
  H142     HC       0.07019     23
  H143     HC       0.07019     24
  H13      HC      -0.05480     25
  C12      ct2      -0.22819     26
  H121     HC       0.02074     27
  H122     HC       0.02074     28
  C11      ct2      0.29696     29
  H111     HC      -0.08535     30
  H112     HC      -0.08535     31
  C10      ct2      -0.16967     32
  H101     HC       0.01763     33
  H102     HC       0.01763     34
  C8       ct1      0.38123     35
  C9       ct3      -0.31498     36
  H91      HC       0.05864     37
  H92      HC       0.05864     38
  H93      HC       0.05864     39
  H8       HC      -0.06230     40
  C7       ct2      -0.27691     41
  H71      HC       0.05395     42
  H72      HC       0.05395     43
  C6       ct2      0.23442     44
  H61      HC      -0.01317     45
  H62      HC      -0.01317     46
  C5       ct2      -0.33480     47
  H51      HC       0.08985     48
  H52      HC       0.08985     49
  C3       cq2      0.21940     50
  C4       ct3      -0.23434     51
  H41      HC       0.08186     52
  H42      HC       0.08186     53
  H43      HC       0.08186     54
  C2       cqq      -0.46505     55
  H2       HA       0.18728     56
  C1       ct2      0.29369     57

```

H11	HC	0.03319	58
H12	HC	0.03319	59
O2A	o1c	-0.48504	60
CGA	c2a	0.90692	61
O1A	o2c	-0.59685	62
CBA	ct2	-0.46156	63
HBA1	HC	0.12241	64
HBA2	HC	0.12241	65
CAA	ct2	-0.04519	66
HAA1	HC	0.03991	67
HAA2	HC	0.03991	68
C2A	ct1	0.17580	69
H2A	HC	0.05578	70
C3A	ct1	0.15276	71
CMA	ct3	-0.36836	72
HMA1	HC	0.09451	73
HMA2	HC	0.09451	74
HMA3	HC	0.09451	75
H3A	HC	0.01996	76
C4A	ccs	0.25138	77
CHB	cab	-0.40864	78
C1B	crb	0.12523	79
NB	nh	-0.09693	80
C4B	cnb	0.04385	81
C3B	cbb	-0.02531	82
C2B	cbb	0.09630	83
CMB	ct3	-0.24283	84
HMB1	HC	0.08822	85
HMB2	HC	0.08822	86
HMB3	HC	0.08822	87
C6B	c2e	0.6950	88
C7B	ct3	-0.3920	89
OB	o2c	-0.5370	90
H7B1	HC	0.075196	91
H7B2	HC	0.075196	92
HB	hn	0.16372	93
HHB	HA	0.14909	94
NA	ns	-0.28377	95
C1A	ccs	-0.11228	96
CHA	csb	0.12976	97
C4D	cqb	0.01537	98
ND	nh	0.02972	99
HD	hn	0.08885	100
CBD	ct1	-0.67857	101
CGD	c2a	0.82970	102
O1D	o2c	-0.57388	103
O2D	o1c	-0.35614	104
CED	ct3	0.06662	105
HED1	HC	0.05534	106
HED2	HC	0.05534	107
HED3	HC	0.05534	108
HBD	HC	0.24601	109
CAD	c2k	0.75090	110
OBD	o2c	-0.58383	111
C3D	cbb	-0.29487	112
C2D	cbb	0.14152	113
CMD	ct3	-0.27550	114
HMD1	HC	0.09098	115
HMD2	HC	0.09098	116

HMD3	HC	0.09098	117
C1D	cpb	-0.01318	118
CHD	cab	-0.26370	119
HHD	HA	0.21030	120
C4C	ccs	0.22486	121
C3CX	ct1	-0.14940	122
CAC	ct2	0.18449	123
CBC	ct3	-0.10787	124
HBC1	HC	0.02491	125
HBC2	HC	0.02491	126
HBC3	HC	0.02491	127
HAC1	HC	-0.01274	128
HAC2	HC	-0.01274	129
C2CX	ct1	0.08674	130
C5C	ct3	-0.28573	131
H5C1	HC	0.08922	132
H5C2	HC	0.08922	133
H5C3	HC	0.08922	134
NC	ns	-0.31971	135
C1C	ccs	0.11298	136
CHC	cab	-0.21525	137
HHC	HA	0.13603	138
H2CX	HC	0.08674	139
H3CX	HC	-0.14940	140
H7B3	HC	0.075196	141

[bonds]

C19	H191
C19	H192
C19	H193
C19	C18
C18	C20
C18	H18
C18	C17
C20	H201
C20	H202
C20	H203
C17	H171
C17	H172
C17	C16
C16	H161
C16	H162
C16	C15
C15	H151
C15	H152
C15	C13
C13	C14
C13	H13
C13	C12
C14	H141
C14	H142
C14	H143
C12	H121
C12	H122
C12	C11
C11	H111
C11	H112
C11	C10
C10	H101

C10	H102
C10	C8
C8	C9
C8	H8
C8	C7
C9	H91
C9	H92
C9	H93
C7	H71
C7	H72
C7	C6
C6	H61
C6	H62
C6	C5
C5	H51
C5	H52
C5	C3
C3	C4
C3	C2
C4	H41
C4	H42
C4	H43
C2	H2
C2	C1
C1	H11
C1	H12
C1	O2A
O2A	CGA
CGA	O1A
CGA	CBA
CBA	HBA1
CBA	HBA2
CBA	CAA
CAA	HAA1
CAA	HAA2
CAA	C2A
C2A	H2A
C2A	C3A
C2A	C1A
C3A	CMA
C3A	H3A
C3A	C4A
CMA	HMA1
CMA	HMA2
CMA	HMA3
C4A	CHB
C4A	NA
CHB	C1B
CHB	HHB
C1B	NB
C1B	C2B
NB	C4B
NB	HB
C4B	C3B
C4B	CHC
C3B	C2B
C3B	C6B
C2B	CMB
CMB	HMB1

CMB HMB2
CMB HMB3
C6B OB
C6B C7B
C7B H7B1
C7B H7B2
C7B H7B3
NA C1A
C1A CHA
CHA C4D
CHA CBD
C4D ND
C4D C3D
ND HD
ND C1D
CBD CGD
CBD HBD
CBD CAD
CGD O1D
CGD O2D
O2D CED
CED HED1
CED HED2
CED HED3
CAD OBD
CAD C3D
C3D C2D
C2D CMD
C2D C1D
CMD HMD1
CMD HMD2
CMD HMD3
C1D CHD
CHD HHD
CHD C4C
C4C C3CX
C4C NC
C3CX CAC
C3CX C2CX
C3CX H3CX
CAC CBC
CAC HAC1
CAC HAC2
CBC HBC1
CBC HBC2
CBC HBC3
C2CX C5C
C2CX C1C
C2CX H2CX
C5C H5C1
C5C H5C2
C5C H5C3
NC C1C
C1C CHC
CHC HHC

[impropers]

C3	C1	C2	H2
C2	C5	C3	C4

O2A	CBA	CGA	O1A
C2A	CHA	C1A	NA
C3A	CHB	C4A	NA
C1B	C4A	CHB	HHB
C1B	C4B	NB	HB
C4B	C2B	C3B	C6B
C3B	CHC	C4B	NB
C2B	CHB	C1B	NB
CMB	C3B	C2B	C1B
C4D	C1D	ND	HD
CBD	C4D	CHA	C1A
CBD	O2D	CGD	O1D
CBD	C3D	CAD	OBD
CAD	C4D	C3D	C2D
C3D	CHA	C4D	ND
C2D	CHD	C1D	ND
CMD	C1D	C2D	C3D
C1D	C4C	CHD	HHD
C3CX	CHD	C4C	NC
CAC	C2CX	C3CX	C4C
C2CX	CHC	C1C	NC